Applied Catalysis B: Environmental 95 (2010) 327–334

Contents lists available at ScienceDirect

Applied Catalysis B: Environmental

journal homepage: www.elsevier.com/locate/apcatb

Catalytic performance of pillared interlayered clays (PILCs) supported CrCe catalysts for deep oxidation of nitrogen-containing VOCs

Qinqin Huang [a], Shufeng Zuo [a,b], Renxian Zhou [a,*]

[a] Institute of Catalysis, Zhejiang University, Hangzhou 310028, PR China
[b] Institute of Applied Chemistry, Shaoxing University, Shaoxing 312000, PR China

ARTICLE INFO

Article history:
Received 25 September 2009
Received in revised form 26 December 2009
Accepted 14 January 2010
Available online 21 January 2010

Keywords:
Pillared interlayered clays
Supported CrCe catalysts
NVOCs oxidation
Porous structure
Acidity

ABSTRACT

Na-montmorillonite (Na-mmt) and different pillared interlayered clays (Al-PILC, Zr-PILC, Ti-PILC and Al_2O_3/Ti-PILC) supported CrCe catalysts for the deep oxidation of nitrogen-containing VOCs (NVOCs) are synthesized and characterized by a combination of X-ray diffraction, N_2 adsorption/desorption, high resolution transmission electron microscopy, temperature-programmed reduction, temperature-programmed desorption and adsorption capacity tests techniques. The results indicate that a porous structure named "house of cards" forms during the pillaring and calcination processes. Both porous structure and acidity play important roles in deep oxidation of NVOCs. The mesoporous structure and the proper acid sites improve the catalytic activity of supported CrCe catalysts. Among all these catalysts, CrCe/Ti-PILC and CrCe/Al_2O_3/Ti-PILC exhibit higher catalytic activity than other catalysts. N-butylamine and ethylenediamine with $-NH_2$ groups are easier to be destructed may be involved in the stronger adsorption on the acid sites of the catalysts. Much too strong adsorption of ethylenediamine on the acid sites leads to a lower activity compared with n-butylamine. Acetonitrile with C≡N bond and little interaction with acid sites is the most difficult to be decomposed. All the catalysts show a good control quality of NO_x, and the yield of NO_x is limited within 2% during the whole experimental temperature range.

1. Introduction

Volatile organic compounds (VOCs) are a wide ranging class of chemicals consisting of over 300 compounds [1]. VOCs are usually emitted from industrial and commercial processes [2]. They are hazardous to the environment and human health. Such compounds may cause the global warming, destroy the ozone layer and some are carcinogens, mutagens and teratogens [3,4]. Therefore, researchers world-wide are urged to find an effective way to treat these pollutants.

Compared with other techniques, such as adsorption, thermal combustion, photocatalysis and plasma catalytic oxidation, the catalytic oxidation of the pollutants to carbon dioxide and water has been identified a more efficient way to destroy VOCs [5]. Catalytic oxidation is effective especially for low concentration VOCs, as it can treat the effluents at low/moderate temperatures and avoid high energy costs [6–9]. Supported noble metal catalysts, such as Pt and Pd catalysts, are effective for VOCs elimination [10–12]. However, high cost of noble metal catalysts prevents the application. Catalysts with low cost and high activity are demanded. Recently, metal oxide based catalysts such as Cr_2O_3, Co_3O_4, CuO and MnO_x are increasingly applied in combustion systems [13–16]. Although metal oxides based catalysts show relatively lower activity, it is one of the widely used catalysts for deep oxidation of VOCs due to the low cost and good resistance to sulfur, chlorine and so on [17].

Pillared interlayered clays (PILCs) have attracted increased interest since the first inorganic pillared clay mineral was reported in the late 1970s [18,19]. It is a kind of material synthesized by exchanging the interlayered cations of smectites with bulky inorganic polyoxycations, followed by calcination [20]. The frequently used pillaring agents are aluminum, zirconium, titanium, iron, chromium, copper or mixed species [18,20,21–25]. Several of the papers devoted to pillared interlayered clays have reviewed various aspects of the preparation, characterization, or applications of these solids [26,27]. Based on the porosity, thermal stability, acidity and reactivity of PILCs [27,28], it has been widely used as support of catalytic materials [29–33] and applied in several chemical processes, such as purification, sorption-based separation, acid-catalyzed reaction, synthesis of bulk/fine chemicals and reduction of pollutants (selective catalytic reduction of NO_x and catalytic removal of VOCs [21–22,34–36]).

In this paper, Na-montmorillonite (Na-mmt), Al-PILC, Zr-PILC, Ti-PILC and Al_2O_3/Ti-PILC supported CrCe catalysts for the deep

* Corresponding author. Tel.: +86 571 88273290; fax: +86 571 88273283.
E-mail address: zhourenxian@zju.edu.cn (R. Zhou).

0926-3373/$ – see front matter. Crown Copyright © 2010 Published by Elsevier B.V. All rights reserved.
doi:10.1016/j.apcatb.2010.01.011

oxidation of NVOCs are synthesized and characterized by XRD, N_2 adsorption/desorption, HRTEM, H_2-TPR, NH_3-TPD and adsorption capacity tests techniques. The scope is to gain some insight into the relation between the catalytic activity and the properties involving as porous structure, acidity, redox properties and reactant adsorption ability, which may be responsible for increasing catalytic oxidation activity for NVOCs.

2. Experimental

2.1. Initial clay

Initial clay was a calcium montmorillonite (Neimenggu, China) with a composition of SiO_2 (58.84%), Al_2O_3 (16.41%), MgO (5.47%), CaO (2.72%), Fe_2O_3 (4.45%), Na_2O (0.07%) and K_2O (0.12%), of which the cation exchange capacity (CEC) is 108.4 mequiv./100 g of clay.

2.2. Supports preparation

2.2.1. Na-mmt

The Na-mmt was obtained by mixing 1 M NaCl and Ca-mmt (0.1 L NaCl/1 g Ca-mmt) with constant stirring at 60 °C for 3 h. Then the clay was centrifuged and washed with distilled water repeatedly until free of Cl^- [21]. The sample was dried at 110 °C overnight.

2.2.2. Al-PILC

The Al-pillaring solution was prepared by hydrolysis of aqueous $AlCl_3{\cdot}6H_2O$ with NaOH at the ratio of OH/Al = 2.4, which was then added drop-wise to the Na-mmt suspension of 2 wt.%. The reaction mixture was stirred continuously for 3 h at 60 °C. Then it was filtered and washed with distilled water repeatedly until free of Cl^- [21]. The sample was dried at 110 °C overnight.

2.2.3. Zr-PILC

The Zr-pillaring solution, which was prepared by aging $ZrOCl_2$ (1 M) at 80 °C for 2 h, was added drop-wise to the Na-mmt suspension of 1 wt.%. The reaction mixture was stirred continuously for 3 h at 60 °C. Then it was filtered and washed with distilled water repeatedly until free of Cl^-. The sample was dried at 110 °C overnight.

2.2.4. Ti-PILC

The Ti-pillaring solution was prepared by hydrolysis of $Ti(OC_4H_9)_4$ with HNO_3 and the pH value (pH = 2) was adjusted by NaOH. Before the solution was added drop-wise to the Na-mmt suspension of 0.5 wt.%. It was aged for 12 h at room temperature. The reaction mixture was stirred continuously for 3 h at room temperature, then it was filtered and washed with distilled water repeatedly until pH = 7. The sample was dried at 110 °C overnight.

2.2.5. Al_2O_3/Ti-PILC

In order to improve the catalytic activity and the properties of the catalyst, Al_2O_3/Ti-PILC was prepared. The preparation is presented below.

The Al-sol (pH = 8–9) was prepared by hydrolysis of $Al(NO_3)_3{\cdot}9H_2O$ with $NH_3{\cdot}H_2O$. Then non-calcined Ti-PILC powder was added to the Al-sol with constant stirring for 1.5 h and then centrifuged. The content of Al_2O_3 is 6 wt.%. The sample was dried at 110 °C overnight.

2.3. Catalysts preparation

Na-mmt, Al-PILC, Zr-PILC, Ti-PILC and Al_2O_3/Ti-PILC supported CrCe catalysts were prepared by an impregnation method with an aqueous solution of $Cr(NO_3)_3{\cdot}9H_2O$ and $Ce(NO_3)_3{\cdot}6H_2O$ as precursors. All the supports were pre-calcined at 500 °C for 2 h. The impregnated catalysts were dried at 110 °C for 2 h, and then calcined at 500 °C for 2 h. The total content of Cr and Ce was 8 wt.% with a molar ratio of Cr/Ce = 6:1.

2.4. Catalytic activity tests

N-butylamine oxidation was carried out in a microreactor (quartz glass, 6 mm i.d., GC 1690, China) under atmospheric pressure at a gas hourly space velocity (GHSV) of 20,000 h^{-1}. The reactive flow was composed of air (100 mL min^{-1}) and about 1000 ppm of gaseous NVOCs (n-butylamine, ethylenediamine and acetonitrile). The catalyst (0.3 mL, 0.30–0.35 g) was loaded in the catalyst bed. A thermocouple was placed in the inlet of catalyst bed to record reaction temperature and also to control the furnace. NVOCs conversion in the effluent gas was analyzed by on-line gas chromatography. The amount of NO_x (calculated from C_{NO^-}) was examined by spectrophotometry. Yield of NO_x is defined as follows:

$$\text{Yield of } NO_x = \frac{C_{exp}}{C_{theo}} = \frac{C_{NO^-}}{(C_{NVOC}/M_{NVOC}) \times M_{NO_2}} = \frac{C_{NO_2^-} \times M_{NVOC}}{C_{NVOC} \times M_{NO_2}}$$

C_{exp}: concentration of NO_2 detected in the oxidation of NVOCs; C_{theo}: concentration of NO_2 obtained from theoretical calculation; $C_{NO_2^-}$: concentration of NO_2^- detected by spectrophotometry; C_{NVOC}: concentration of NVOC injected to the system before NVOCs oxidation; M_{NO_2}: mole mass of NO_2; M_{NVOC}: mole mass of NVOC.

2.5. Catalysts characterization

2.5.1. N_2 adsorption/desorption

Textural properties of the samples were measured by N_2 adsorption/desorption at liquid nitrogen temperature using a Coulter OMNISORP-100 apparatus. The samples were degassed under vacuum at 200 °C for 2 h before the measurements.

2.5.2. X-ray diffraction (XRD)

The phase composition of these samples was determined by means of X-ray diffraction (XRD), using a RigakuD/max-3BX. The operating parameters were as follows: monochromatic Cu Kα radiation, Ni filter, 40 mA, 40 kV, 2θ values between 0.5° and 80°.

2.5.3. High resolution transmission electron microscopy (HRTEM)

Surface morphology analysis was carried out using high resolution transmission electron microscopy (HRTEM) on a JEM-2010 apparatus operated at 200 kV. The samples were pre-treated by epon embedding and ultra-thin sectioning.

2.5.4. Temperature-programmed reduction of H_2 (H_2-TPR)

The temperature-programmed reduction of H_2 (H_2-TPR) was performed in a quartz fixed-bed microreactor (i.d. = 6 mm) equipped with TCD. Prior to H_2-TPR measurement, the catalyst (100 mg) was pre-treated in air stream at 300 °C for 0.5 h. After being cooled down to 50 °C in the same atmosphere, the sample was exposed to a flow (40 mL min^{-1}) of 5 vol.% H_2/Ar and heated to 900 °C with a heating rate of 10 °C min^{-1}.

2.5.5. Temperature-programmed desorption of NH_3 (NH_3-TPD)

The temperature-programmed desorption of NH_3 (NH_3-TPD) was performed in a quartz fixed-bed microreactor (i.d. = 6 mm) equipped with TCD. Prior to NH_3-TPD measurement, the catalyst (100 mg) was pre-treated in an Ar stream at 500 °C for 0.5 h. After being cooled down to 100 °C, the catalyst was exposed to a flow of NH_3 (20 mL min^{-1}) stream for 0.5 h, and then treated in Ar (99.99%, 40 mL min^{-1}) for 1.5 h in order to remove physically bound

ammonia. Finally desorption performance was carried out from 100 to 500 °C with a heating rate of 10 °C min^{-1}.

2.5.6. Adsorption capacity tests

The adsorption capacity of n-butylamine over these catalysts was carried out in a quartz fixed-bed microreactor (i.d. = 6 mm) to determine the relationship between catalytic activity and structure properties. The catalyst (100 mg) was pre-treated in Ar (99.99%) at 450 °C for 1 h. After being cooled down to 50 °C, the catalyst was exposed to a flow air stream (100 mL min^{-1}) containing about 1000 ppm n-butylamine. The outlet gases were analyzed on-line over a mass spectrometer apparatus (Hiden QIC-20).

3. Results and discussion

3.1. Catalytic activity results

The light-off curves of n-butylamine oxidation over supported CrCe catalysts are displayed in Fig. 1. The catalytic activity depends on the properties of supports. CrCe/Na-mmt shows the lowest catalytic activity, while the activity of CrCe/PILC catalysts is improved evidently, especially for CrCe/Ti-PILC and CrCe/Al_2O_3/Ti-PILC. On the basis of T_{50}, the catalytic activity of the catalysts decreases in the order: CrCe/Al_2O_3/Ti-PILC (170 °C) > CrCe/Ti-PILC (180 °C) > CrCe/Zr-PILC (210 °C) > CrCe/Al-PILC (240 °C) > CrCe/Na-mmt (260 °C).

In the literature reported previously, the processes of the oxidation of NVOCs occurred via a similar mechanism, proposed as the following general scheme (Fig. 2) [37]. It is evidently known that N_2 and NO_x are common nitrogen-containing products during deep oxidation of NVOCs. It has important meaning to control formation of NO_x for deep oxidation of NVOCs, so the yield of NO_x is also measured to confirm the catalytic activity of the supported CrCe catalysts. The NO_x yield during n-butylamine deep oxidation is presented in Fig. 3. It can be observed that the yield of NO_x for all the catalysts is low at T_{98}. And the yield stays below 2% even the reaction temperature increases by 50 °C, which means minority of NO_x is produced during n-butylamine oxidation. The results suggest that all the supported CrCe catalysts show a good control quality of NO_x.

Based on the high activity and easy preparation, CrCe/Ti-PILC is chosen to evaluate the deep oxidation performance of various NVOCs. Light-off curves for deep oxidation of various NVOCs over CrCe/Ti-PILC are shown in Fig. 4. All the NOVCs can be completely destructed on CrCe/Ti-PILC, but different activities are obtained. The difference is more evident at lower temperatures but the gap gradually narrows down as the temperature increases until total conversion is attained. The difference in the activity may be due to the characters of the reactants. N-butylamine and ethylenediamine with $-NH_2$ groups show a strong adsorption on acid sites of the catalysts than acetonitrile. As a consequence, a partial positive charge center forms on the carbon atom and can act as electrophilic site in the combustion reactions [38]. However, it is supposed that ethylenediamine with more alkalinity exhibits much too strong adsorption on the acid sites, which may go against its desorption and further oxidation. So ethylenediamine shows a lower catalytic activity of in comparison with n-butylamine. The lowest activity of acetonitrile may be due to the C≡N bond as well as lack of a strong interaction with acid site of the catalysts. The trend of NO_x yield is opposite from the conversion of these NVOCs,

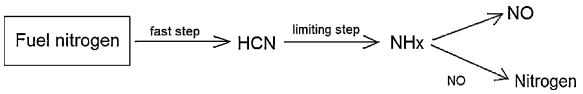

Fig. 2. Scheme for the mechanism of NVOCs conversion.

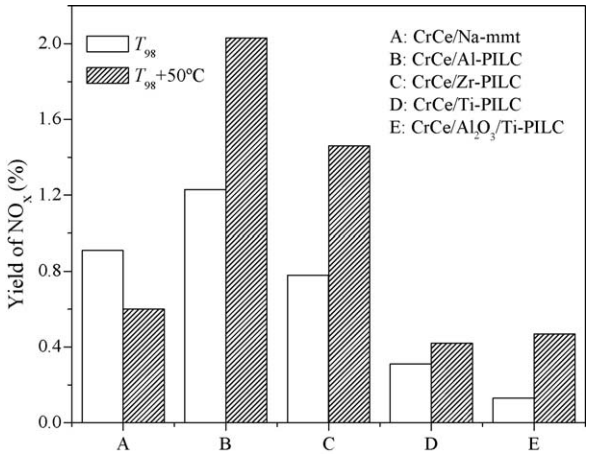

Fig. 3. NO_x yield over supported CrCe catalysts.

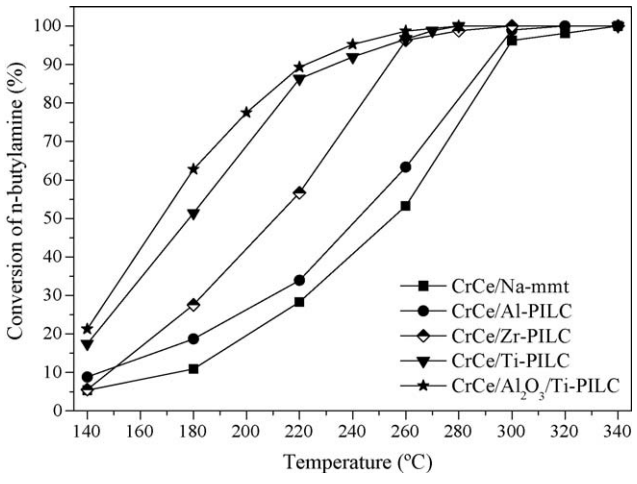

Fig. 1. Light-off curves for deep oxidation of n-butylamine over supported CrCe catalysts.

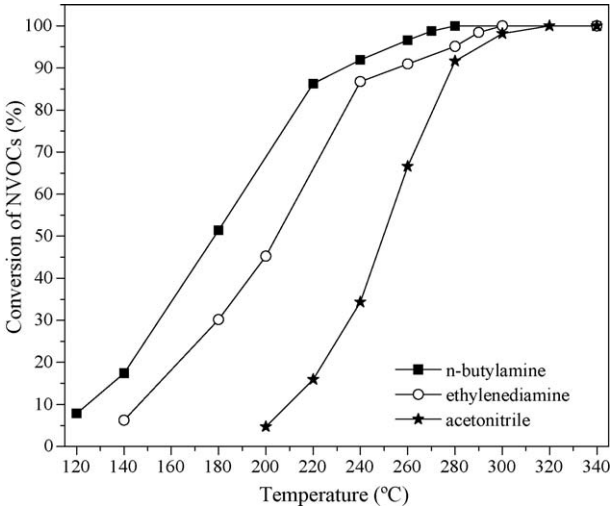

Fig. 4. Light-off curves for deep oxidation of various NVOCs over CrCe/Ti-PILC.

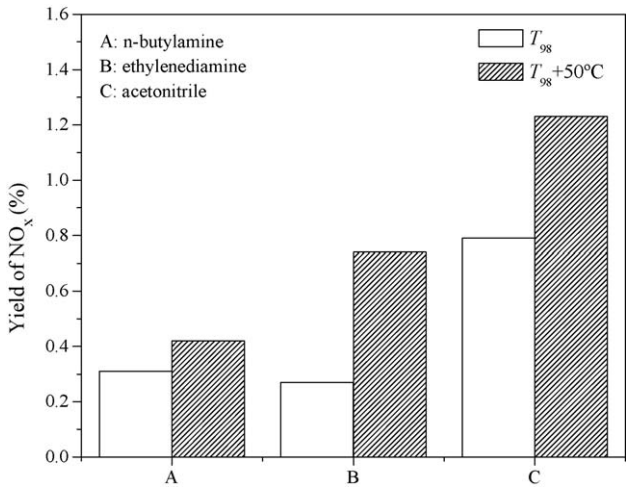

Fig. 5. NO_x yield of various NVOCs over CrCe/Ti-PILC.

because the amount of NO_x depends on the nitrogen contained in the compound and the experimental temperature. For all these reactants, the yield of NO_x is limited within 2% during the whole temperature range (shown in Fig. 5).

3.2. Characterization results

3.2.1. N_2 adsorption/desorption results

N_2 adsorption/desorption isotherms and pore distribution of the supported CrCe catalysts are displayed in Fig. 6. The data of surface area and pore volume are listed in Table 1. All the adsorption isotherms and hysteresis loops of supported CrCe catalysts seem to be of type IV and type H_3 according to IUPAC classification [39]. In all isotherms, the desorption branch shows an inflection "knee" at about 0.45–0.50P/P_0, which has been observed for many different types of layered materials when nitrogen is used as the adsorbent gas (nitrogen boils at P/P_0 0.42) [40–42]. It is sometimes called the tensile strength artifact due to the complexity of capillary condensation in pore networks with pore blocking effects [43]. A narrow distribution of micropores with a diameter less than 1.2 nm and mesopores with a diameter of about 3.85–3.89 nm are observed for the supported CrCe catalysts.

As is reported in Table 1, all the PILCs show a visible increase in both surface area and pore volume comparing with that of Na-mmt. For the PILCs, the surface area is about 160–220 m^2/g and the pore volume reaches about 0.14–0.20 cm^3/g. The increase of pore volume of Al-PILC and Zr-PILC is mainly due to micropores creation while that of Ti-PILC and Al_2O_3/Ti-PILC is ascribed to both micropores and mesopores exhibition. However, since the porous structure is blocked by some of the active phases after deposition of chromium and cerium on these supports, the surface area and pore volume of the supported CrCe catalysts decrease evidently.

Table 1
Surface area and pore volume of supports and supported CrCe catalysts.

	S_{BET} (m^2/g)[a]	V_{mic} (cm^3/g)[b]	V_{mes} (cm^3/g)[c]	V_T (cm^3/g)
Supports				
Na-mmt	62	0.021	0.099	0.120
Al-PILC	217	0.087	0.096	0.183
Zr-PILC	167	0.066	0.075	0.141
Ti-PILC	207	0.068	0.130	0.198
Al_2O_3/Ti-PILC	196	0.067	0.112	0.177
Catalysts				
CrCe/Na-mmt	60	0.020	0.089	0.111
CrCe/Al-PILC	125	0.047	0.071	0.118
CrCe/Zr-PILC	114	0.042	0.078	0.120
CrCe/Ti-PILC	183	0.060	0.107	0.167
CrCe/Al_2O_3/Ti-PILC	163	0.058	0.089	0.144

[a] Calculated from BET surface area and the range of P/P_0 used is from 0.05 to 0.25.
[b] Calculated from HK method.
[c] Calculated from BJH method.

It has been reported in the previous literature [6,44] that the structure of PILCs has a marked effect on the activity for deep oxidation of VOCs. Xia et al. [45] found that the catalytic activity for aromatics oxidation is dependent on the pore size. As there is a smaller resistance for diffusion of reactants/products in and out of the larger pores, leading to higher catalytic activity. According to our results of catalytic activity tests and N_2 adsorption/desorption, it is also suggested that the catalysts with larger surface area and more mesoporous structure exhibit better catalytic activity. The results obtained by other researchers are as well fit for deep oxidation of n-butylamine.

3.2.2. XRD results

XRD patterns of the supported CrCe catalysts are presented in Fig. 7. Distinct diffraction peaks of Cr_2O_3 [46] are observed on all the catalysts. The diffraction peak at about 25.5°, which exhibits only in CrCe/Ti-PILC and CrCe/Al_2O_3/Ti-PILC catalysts, is ascribed to anatase TiO_2 [47]. And the peak appearing at about 28.2° is assigned as a combined signal of CeO_2 and montmorillonite [48,49], since weak signal of low content CeO_2 may be overlapped by the montmorillonite signal.

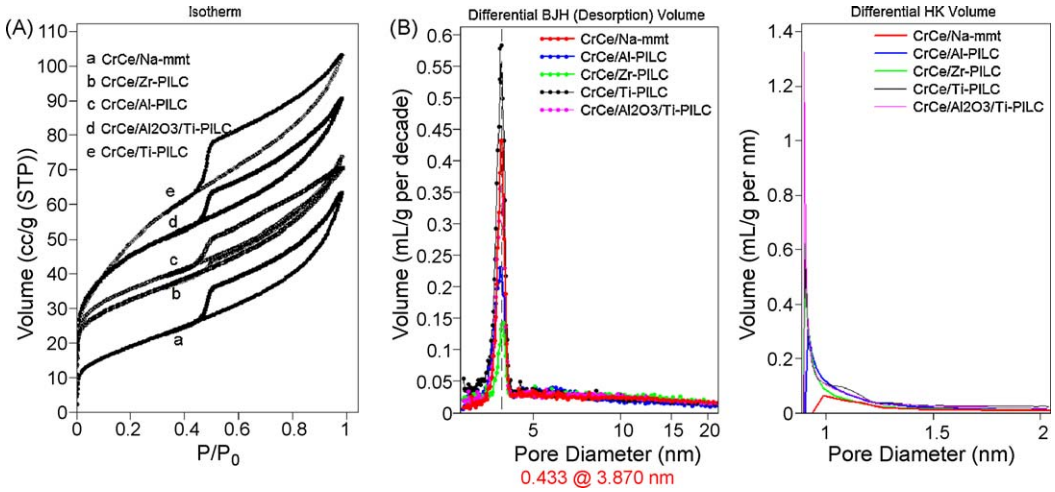

Fig. 6. (A) The isotherms and (B) pore distribution of supported CrCe catalysts.

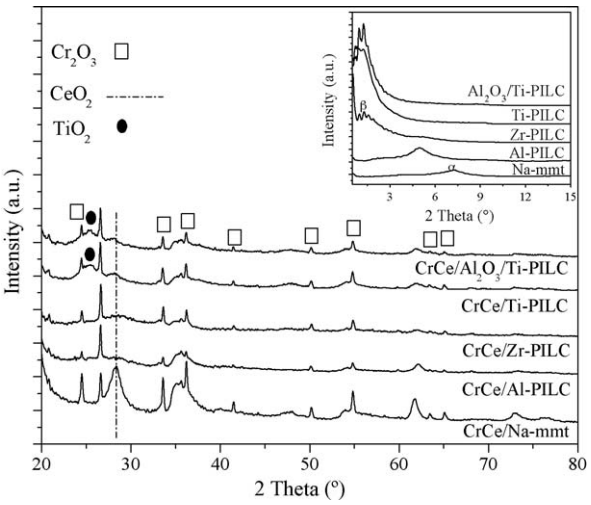

Fig. 7. XRD patterns of supported CrCe catalysts (inset figure: XRD patterns of supports between 0.5° and 15°).

It is known that certain supports favor the production of crystallites by the transition metal oxides. Bond and Tahir [50] and Bertinchamps et al. [51] reported that at the opposite of titanias, Al_2O_3 and SiO_2 prevented the homogeneous spreading of the active phase but promoted the formation of poorly dispersed crystallites of active phase. It is also reported in previous literature that the Lewis sites presented on PILCs promoted the dispersion of the active phases [16,50–53]. In our study, it is found that the intensity of diffraction peaks of active phases in CrCe/PILC catalysts is much lower than that in CrCe/Na-mmt. So, it is deduced that PILCs with larger surface area, more pore volume and Lewis sites are in favor of better dispersion of active phases.

Low angles XRD patterns (between 0.5° and 15°) of Na-mmt and four PILCs are presented in the inset figure of Fig. 7. The diffraction peak (peak α) corresponding to the diffraction of periodic is detected in Na-mmt ($d_{0\,0\,1} \approx 1.21$ nm), Al-PILC ($d_{0\,0\,1} \approx 1.78$ nm) and Zr-PILC ($d_{0\,0\,1} \approx 1.71$ nm). It is similar to the results obtained by other researchers, who ascribed this considerable enhancement of $d_{0\,0\,1}$ to the intercalation of alumina species [21,22] or zirconium species. However, not peak α but intensive diffraction peaks (peak β) are observed at lower angles at about 1° or even below in Ti-PILC and Al_2O_3/Ti-PILC, which is also detected in Zr-PILC. The results are analogous to previously observation in Zr-PILC and Ti-PILC, which is attributed to a highly disordered structure [54,55]. Mandalia et al. prepared Fe_2O_3-PILC with a $d_{0\,0\,1}$ of 7.2 nm, and proposed that the result cannot be assigned to simple intercalation of iron hydroxycations [56,57], but to the existence of some porous structure. Indeed, some disordered solids show broad XRD peak at very low 2θ angles, such as porous silica [58], silica molecular sieves [59] and mesoporous biogenetic silica [60]. Based on the discussion above, the diffraction peaks of Zr-PILC, Ti-PILC and Al_2O_3/Ti-PILC appearing at the very low angles may be correlated with some disordered porous structure, rather than large interlayer distances of PILCs.

3.2.3. HRTEM results

As shown in HRTEM results (Fig. 8), Na-mmt has a two-dimensional porous structure with a small interlayer distance. After pillaring and calcination processes, the interlayer distance is enlarged, remaining the regular layer structure in Al-PILC. However, such regular structure collapses in Zr-PILC (partially), Ti-PILC (completely) and Al_2O_3/Ti-PILC (completely), leading to the overlap of clay layers.

Combining with the results of N_2 adsorption/desorption, XRD and HRTEM, we conclude that pillaring and calcination processes result in collapse of layer structure. And then the fragments of PILCs together with inorganic polyoxocations reforms a wholly different structure, defined as "house of cards" [61]. The "house of cards" structure may form in every step of PILCs synthesis. During the pillaring process, the clay structure can be influenced as a consequence of pillaring agent used [62] or pH values attained [63]. In the process of drying, the method used has an effect on the structure of pillared clays [64]. During the calcination, "house of cards" can also be produced due to the collapse of the clay layers [46]. Further more, the nature of the clay can also lead to the production such structure. For instance, a synthetic hectorite with a relatively small layer aspect ratio has a high tendency to form "house of cards" structure [65]. The formation of "house of cards" in our study can be explained briefly as follows: Na-mmt is modified by introducing large inorganic polyoxocations into interlayer regions. The polyoxocations enlarge the interlayer

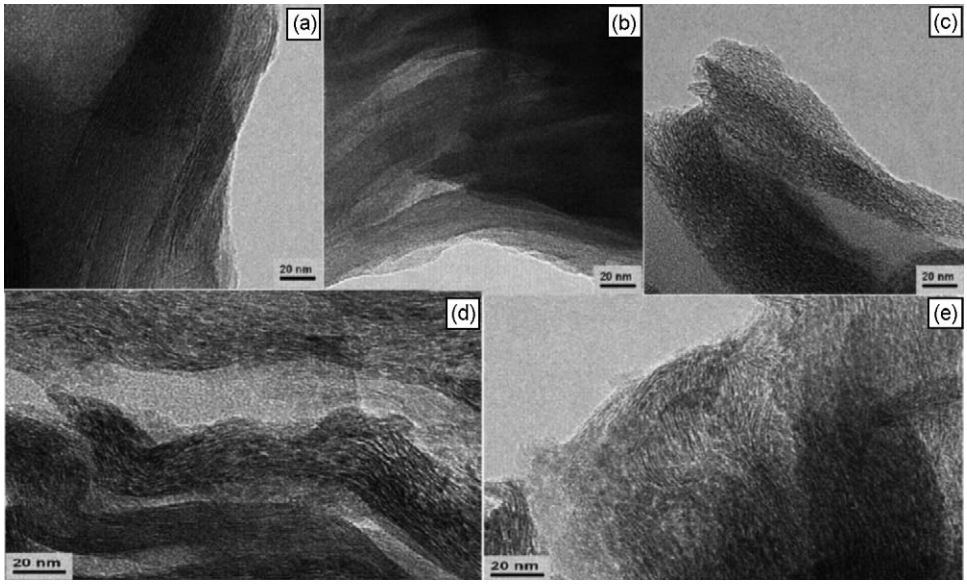

Fig. 8. HRTEM images of supports (a) Na-mmt, (b) Al-PILC, (c) Zr-PILC, (d) Ti-PILC and (e) Al_2O_3/Ti-PILC.

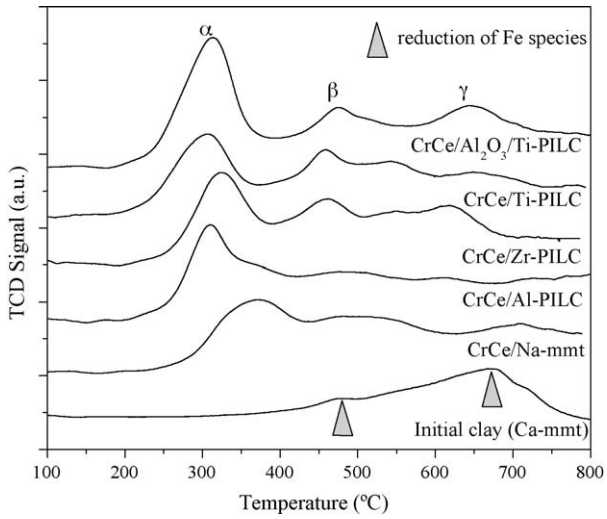

Fig. 9. H_2-TPR profiles of Ca-mmt (the original clay) and supported CrCe catalysts.

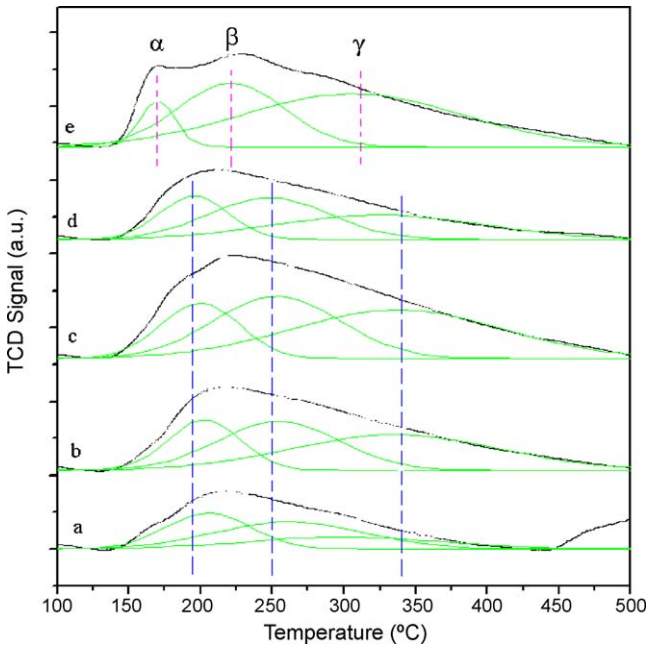

Fig. 10. NH_3-TPD profiles of supported CrCe catalysts (a) CrCe/Na-mmt, (b) CrCe/Al-PILC, (c) CrCe/Zr-PILC, (d) CrCe/Ti-PILC and (e) CrCe/Al_2O_3/Ti-PILC.

distance of the clay. After calcination process, these polyoxocations convert to metal oxide clusters and the clay layers collapse. Finally, a different porous structure forms.

3.2.4. H_2-TPR results

H_2-TPR profiles of the original clay and the supported CrCe catalysts are shown in Fig. 9. The reduction of Fe species is obviously observed in the initial clay (Ca-mmt), which is caused by the relatively high content of Fe_2O_3 (4.45% in the original clay) [66,67]. Three hydrogen consumption peaks (peaks α, β and γ) are detected on all the supported catalysts. According to the literature reported, there are two H_2 consumption peaks during reduction of Cr_2O_3 [68,69], and ceria can be reduced by H_2 only at temperature higher than 350 °C [70–73]. As a result, the intense peak α is ascribed to the reduction of Cr_2O_3, while peak β is a combined reduction of Cr species, ceria together with Fe species. Peak γ may be the reduction of Fe species together with ceria.

Focusing on peak α, the area of which decreases as follows: CrCe/Al_2O_3/Ti-PILC > CrCe/Ti-PILC > CrCe/Zr-PILC > CrCe/Al-PILC > CrCe/Na-mmt. Although XRD characterization does not reveal intensive diffraction peaks of Cr_2O_3 on CrCe/PILCs catalysts as that on CrCe/Na-mmt, Cr_2O_3 clusters are confirmed to be present in a highly dispersion form on the four PILCs according to the H_2-TPR results [74]. The peak-temperature of peak α decreases in the order: CrCe/Na-mmt (370 °C) > CrCe/Zr-PILC (325 °C) > CrCe/Al_2O_3/Ti-PILC (310 °C), CrCe/Ti-PILC (310 °C), CrCe/Al-PILC (310 °C). It is obviously seen that peak α of the CrCe/PILCs catalysts shifts to a lower temperature range compared with that of CrCe/Na-mmt, indicating the properties of PILCs have a positive effect on the interaction between Cr_2O_3 and CeO_2, which is beneficial to the migration of bulk oxygen of ceria and further promotes the catalytic activity of the catalysts [71].

3.2.5. NH_3-TPD results

As is reported in previous studies, the acidity of the catalysts plays an important role in the adsorption and oxidation of VOCs. NH_3-TPD is a most widely used method for characterizing acidity of catalysts. And the NH_3 desorbed above 100 °C is considered as chemisorbed NH_3, which is subsequently used for acidity determination [3,4,75].

NH_3-TPD profiles of the supported CrCe catalysts are exhibited in Fig. 10. The peak-temperature of desorption peak of each catalyst is reported in Table 2. All the catalysts show three

Table 2
Peak-temperature of desorption peaks of supported CrCe catalysts.

	Peak α (°C)	Peak β (°C)	Peak γ (°C)
CrCe/Na-mmt	206	262	312
CrCe/Al-PILC	199	256	341
CrCe/Zr-PILC	199	255	348
CrCe/Ti-PILC	192	249	348
CrCe/Al_2O_3/Ti-PILC	170	220	312

desorption peaks in the experimental temperature range. They are classified as weak acidity, medium acidity and strong acidity according to the temperature range in which most ammonia is desorbed. However, CrCe/Al_2O_3/Ti-PILC displays lower peak-temperature of desorption peaks, about 170, 220 and 312 °C,

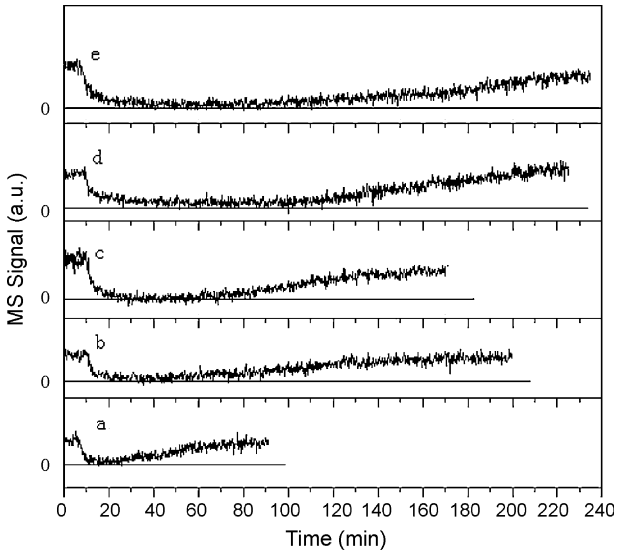

Fig. 11. N-butylamine adsorption capacity profiles of supported CrCe catalysts (a) CrCe/Na-mmt, (b) CrCe/Al-PILC, (c) CrCe/Zr-PILC, (d) CrCe/Ti-PILC and (e) CrCe/Al_2O_3/Ti-PILC.

Table 3
N-butylamine adsorption capacity of supported CrCe catalysts.

Catalyst	Adsorption time[a] (min)	N-butylamine[b] adsorption capacity (mmol/g cat.)
CrCe/Na-mmt	70	0.81
CrCe/Al-PILC	160	1.85
CrCe/Zr-PILC	148	1.71
CrCe/Ti-PILC	205	2.37
CrCe/Al_2O_3/Ti-PILC	217	2.51

[a] Approximate time.
[b] A flow (100 mL min^{-1}) containing about 1000 ppm of gaseous n-butylamine.

indicating that it has relatively weaker acidity. As is known, the amount of NH_3 desorbed is taken as a measure of the acid sites concentration. It is evident that the order of the overall acidity resulted to be: CrCe/Na-mmt ≪ CrCe/Al-PILC, CrCe/Ti-PILC < CrCe/Zr-PILC < CrCe/Al_2O_3/Ti-PILC. Combining with the catalytic activity results, we suggest that catalysts with suitable number of relatively weaker acidity are fit for adsorption and deep oxidation of n-butylamine.

3.2.6. Adsorption capacity results

The adsorption capacity curves of n-butylamine over different supported CrCe catalysts are shown in Fig. 11. The values of adsorption capacity of each catalyst are listed in Table 3. The adsorption capacity of each catalyst follows the order: CrCe/Al_2O_3/Ti-PILC > CrCe/Ti-PILC > CrCe/Al-PILC > CrCe/Zr-PILC ≫ CrCe/Na-mmt, which demonstrates that PILCs exhibit more adsorption capacity due to lager surface area, more mesopore volume and more weak acid sites. Further more, according to the activity tests, it is suggested that catalyst with lager adsorption capacity reveals better catalytic activity.

4. Conclusion

The catalytic activity of Na-mmt and PILCs supported CrCe catalysts for deep oxidation of NVOCs is studied. According to the characterization results of these catalysts, it is concluded that a porous structure defined as "house of cards" resulting from the overlap of clay layers forms during the pillaring and calcination processes. The increase of pore volume in PILCs is beneficial to the dispersion of active phases. Both porous structure and acidity of catalysts play important roles in deep oxidation of NVOCs. Catalysts with mesoporous structure and proper acid sites display larger adsorption capacity of reactant, which promote the activity of the catalysts. The catalytic activity of these catalysts decreases in the order: CrCe/Al_2O_3/Ti-PILC > CrCe/Ti-PILC > CrCe/Zr-PILC > CrCe/Al-PILC > CrCe/Na-mmt. Among the three NVOCs, n-butylamine and ethylenediamine with $-NH_2$ group are easier to be adsorbed on the acid sites of the catalyst. So they are more easily to be destructed. But much too strong adsorption of ethylenediamine on the acid sites leads to a lower activity compared with n-butylamine. Acetonitrile with C≡N bond and little interaction with acid sites is the most difficult to be decomposed. All the catalysts exhibit good control quality of NO_x, limiting the NO_x yield within 2%.

Acknowledgements

We gratefully acknowledge the financial supports from the Ministry of Science and Technology of China (No. 2004 CB 719504) and Nature Science Foundation of China (No. 20577043).

References

[1] S.H. Taylor, C.S. Heneghan, G.J. Hutchings, I.D. Hudson, Catal. Today 59 (2000) 249–259.
[2] E. Noordally, J.R. Richmond, S.F. Tahir, Catal. Today 17 (1993) 359–366.
[3] R. López-Fonseca, A. Aranzabal, J.I. Gutiérrez-Ortiz, J.I. Álvarez-Uriarte, J.R. González-Velasco, Appl. Catal. B: Environ. 30 (2001) 303–313.
[4] R. López-Fonseca, A. Aranzabal, P. Steltenpohl, J.I. Gutiérrez-Ortiz, J.R. González-Velasco, Catal. Today 62 (2000) 367–377.
[5] M. Labaki, S. Siffert, J.-F. Lamonier, E.A. Zhilinskaya, A. Aboukaïs, Appl. Catal. B: Environ. 43 (2003) 261–271.
[6] S.F. Zuo, Q.Q. Huang, R.X. Zhou, Catal. Today 139 (2008) 88–93.
[7] J.J. Spivey, Ind. Eng. Chem. Res. 26 (1987) 2165–2180.
[8] J.N. Armor, Appl. Catal. B: Environ. 1 (1992) 221–256.
[9] J.J. Spivey, J.B. Butt, Catal. Today 11 (1992) 465–500.
[10] J.-M. Giraudon, A. Elhachimi, G. Leclercq, Appl. Catal. B: Environ. 84 (2008) 251–261.
[11] L.F. Wang, M. Sakurai, H. Kameyama, J. Hazard. Mater. 154 (2008) 390–395.
[12] B. Grib, N. Radic, Z. Arsenijevic, R. Garic-Grulovic, Z. Grbavcic, Appl. Catal. B: Environ. 90 (2009) 478–484.
[13] L. Storato, R. Ganzerla, M. Lenarda, R. Zanoni, A.J. López, P. Olivera-Pastor, E.R. Castellón, J. Mol. Catal. A: Chem. 115 (1997) 329–338.
[14] S. Krishnamoorthy, J.A. Rivas, M.D. Amiridis, J. Catal. 193 (2000) 264–272.
[15] D. Delimaris, T. Ioannides, Appl. Catal. B: Environ. 89 (2009) 295–302.
[16] S.F. Zuo, Q.Q. Huang, J. Li, R.X. Zhou, Appl. Catal. B: Environ. 91 (2009) 204–209.
[17] J.I. Gutiérrez-Ortiz, B. de Rivas, R. López-Fonseca, S. Martín, J.R. González-Velasco, Chemosphere 68 (2007) 1004–1012.
[18] P. Yuan, F. Annabi-Bergaya, Q. Tao, M.D. Fan, Z.W. Liu, J.X. Zhu, H.P. He, T.H. Chen, J. Colloid Interface Sci. 324 (2008) 142–149.
[19] G.W. Brindley, R.E. Sempels, Clay Miner. 12 (1977) 229–237.
[20] M. Sychev, R. Prihod'ko, A. Stepanenko, M. Rozwadowski, V.H.J. (San) de Beer, R.A. van Santen, Micropor. Mesopor. Mater. 47 (2001) 311–321.
[21] S.F. Zuo, R.X. Zhou, Appl. Surf. Sci. 253 (2006) 2508–2514.
[22] S.F. Zuo, R.X. Zhou, Micropor. Mesopor. Mater. 113 (2008) 472–480.
[23] S.V. Awate, S.B. Waghmode, M.S. Agashe, Catal. Commun. 5 (2004) 407–411.
[24] R.Q. Long, R.T. Yang, Appl. Catal. B: Environ. 27 (2000) 87–95.
[25] S. Caudo, G. Centi, C. Genovese, S. Perathoner, Appl. Catal. B: Environ. 70 (2007) 437–446.
[26] A. Gil, S.A. Korili, M.A. Vicente, Catal. Rev. 50 (2008) 153–221.
[27] G. Centi, S. Perathoner, Micropor. Mesopor. Mater. 107 (2008) 3–15.
[28] T.J. Pinnavaia, Science 220 (1983) 365–371.
[29] S. Cheng, Catal. Today 49 (1999) 303–312.
[30] A. Gil, L.M. Gandia, M.A. Vicente, Catal. Rev. Sci. Eng. 42 (2000) 145–212.
[31] E.M. Serwicka, K. Bahranowski, Catal. Today 90 (2004) 85–92.
[32] A. De Stefanis, A.A.G. Tomlinson, Catal. Today 114 (2006) 126–141.
[33] D.M. Manohar, B.F. Noeline, T.S. Anirudhan, Appl. Clay Sci. 31 (2006) 194–206.
[34] A. Bahamonde, F. Mohino, M. Rebollar, M. Yates, P. Avila, S. Mendioroz, Catal. Today 69 (2001) 233–239.
[35] H.J. Chae, I.-S. Nam, S.-W. Ham, S.B. Hong, Appl. Catal. B: Environ. 53 (2004) 117–126.
[36] N. Sanabria, A. Álvarez, R. Molina, S. Moreno, Catal. Today 133 (2008) 530–533.
[37] Z.R. Ismagikov, M.A. Kerzhensev, Catal. Rev. Sci. Eng. 32 (1990) 51–103.
[38] A.Z. Abdullah, B.Z.A. Bakar, S. Bhatia, J. Hazard. Mater. B129 (2006) 39–49.
[39] S.J. Gregg, K.S.W. Sing, Adsorption, Surface Area and Porosity, second ed., Academic Press, New York, 1982.
[40] P. Cool, H.Y. Zhu, K. Cassiers, E.F. Vansant, Stud. Surf. Sci. Catal. 154 (2004) 789–796.
[41] S.M. Auerbach, K.A. Carrado, P.K. Dutta, Handbook of Layered Materials, Marcel Dekker, New York, 2004.
[42] P. Yuan, H.P. He, F. Bergaya, D.Q. Wu, Q. Zhou, J.X. Zhu, Micropor. Mesopor. Mater. 88 (2006) 8–15.
[43] K.S.W. Sing, D.H. Everett, R.A.W. Haul, L. Moscou, R.A. Pierotti, J. Rouquerol, T. Siemieniewska, Pure Appl. Chem. 57 (1985) 603–619.
[44] A. Gil, M.A. Vicente, J.-F. Lambert, L.M. Gandía, Catal. Today 68 (2001) 41–51.
[45] Q.-H. Xia, K. Hidajat, S. Kawi, Catal. Today 68 (2001) 255–262.
[46] D.H. Cho, Y.G. Kim, M.J. Chung, J.S. Chung, Appl. Catal. B: Environ. 18 (1998) 251–261.
[47] V. Belessi, D. Lambropoulou, I. Konstantinou, A. Katsoulidis, P. Pomonis, D. Petridis, T. Albanis, Appl. Catal. B: Environ. 73 (2007) 292–299.
[48] X.-S. Huang, H. Sun, L.C. Wang, Y.-M. Liu, K.-N. Fan, Y. Cao, Appl. Catal. B: Environ. 90 (2009) 224–232.
[49] L. Chmielarz, P. Kuśtrowsik, M. Zbroja, A. R-Łasocha, B. Dudek, R. Dziembaj, Appl. Catal. B: Environ. 45 (2003) 103–116.
[50] G.C. Bond, S.F. Tahir, Appl. Catal. 71 (1991) 1–31.
[51] F. Bertinchamps, C. Grégoire, E.M. Gaigneaux, Appl. Catal. B: Environ. 66 (2006) 1–9.
[52] D. Jerónimo, J.M. Guil, B.M. Corbella, H. Vasques, A. Miranda, J.M. Silva, A. Lobato, J. Pires, A.P. Carvalho, Appl. Catal. A: Gen. 330 (2007) 89–95.
[53] F. Figueras, Catal. Rev. Sci. Eng. 30 (1988) 457–499.
[54] P. Yuan, X.L. Yin, H.P. He, D. Yang, L.J. Wang, J.X. Zhu, Micropor. Mesopor. Mater. 93 (2006) 240–247.
[55] M.R.S. Kou, S. Mendioroz, M.I. Guijarro, Thermochim. Acta 323 (1998) 145–157.
[56] C. Clinard, T. Mandalia, D. Tchoubar, F. Bergaya, Clays Clay Miner. 51 (2003) 421–429.
[57] T. Mandalia, M. Crespin, D. Messad, F. Bergaya, Chem. Commun. 19 (1998) 2111–2112.
[58] P. Levitz, D. Tchoubar, J. Phys. 2 (1992) 771–790.
[59] S.A. Bagshaw, E. Prouzet, T.J. Pinnavaia, Science 269 (1995) 1242–1244.
[60] C.E. Fowler, Y. Hoog, L. Vidal, B. Lebeau, Chem. Phys. Lett. 398 (2004) 414–417.
[61] D.E.W. Vaughan, R.J. Lussier, Prepr. 5th Int. Conf. Zeolites, Naples, 1980.
[62] M.N. Timofeeva, S.Ts. Khankhasaeva, S.V. Badmaeva, A.L. Chuvilin, E.B. Burgina, A.B. Ayupov, V.N. Panchenko, A.V. Kulikova, Appl. Catal. B: Environ. 59 (2005) 243–248.

[63] E.M. Farfan-Torres, E. Sham, P. Grange, Catal. Today 15 (1992) 515–526.
[64] T.J. Pinnavala, M.-S. Tzou, S.D. Landau, R.H. Raythatha, J. Mol. Catal. 27 (1984) 195–212.
[65] V. Belessi, D. Lambropoulou, I. Konstantinou, A. Katsoulidis, P. Ponomis, D. Petridis, T. Albanis, Appl. Catal. B: Environ. 73 (2007) 292–299.
[66] W.K. Jóźwiak, J. Góralski, F. Domka, Appl. Catal. A: Gen. 190 (2000) 107–115.
[67] F.G. Durán, B.P. Barbero, L.E. Cadús, C. Rojas, M.A. Centeno, J.A. Odriozola, Appl. Catal. B: Environ. 92 (2009) 194–201.
[68] J. Słoczyński, J. Janas, T. Machej, J. Rynkowski, J. Stoch, Appl. Catal. B: Environ. 24 (2000) 45–60.
[69] C.M. Pradier, F. Rodrigues, P. Marcus, M.V. Landau, M.L. Kaliya, A. Gutman, M. Herskowitz, Appl. Catal. B: Environ. 27 (2000) 73–85.
[70] T. Caputo, L. Lisi, R. Pirone, G. Russo, Appl. Catal. A: Gen. 348 (2008) 42–53.
[71] M. Primet, E. Garbowski, in: A. Trovarelli (Ed.), Catalysis by Ceria and Related Materials, Catalysis Science Series, vol. 2, Imperial College Press, London, 2002.
[72] A. Pintar, J. Batista, S. Hočevar, J. Colloid Interface Sci. 285 (2005) 218–231.
[73] P. Ratnasamy, D. Srinivas, C.V.V. Satyanarayana, P. Manikandan, R.S. Senthil Kumaran, M. Sachin, V.N. Shetti, J. Catal. 221 (2004) 455–465.
[74] J.I. Gutiérrez-Oritz, R. López-Fonseca, U. Aurrekoetxea, J.R. González-Velasco, J. Catal. 218 (2003) 148–154.
[75] J.M. Zhou, L. Zhao, Q.Q. Huang, R.X. Zhou, X.K. Li, Catal. Lett. 127 (2009) 277–284.